# System Identification of Alfred Zampa Memorial Bridge Using Dynamic Field Test Data

Xianfei He[1]; Babak Moaveni, A.M.ASCE[2]; Joel P. Conte, M.ASCE[3]; Ahmed Elgamal, M.ASCE[4]; and Sami F. Masri, M.ASCE[5]

**Abstract:** The Alfred Zampa Memorial Bridge (AZMB), a newly built long-span suspension bridge, is located 32 km northeast of San Francisco on interstate Highway I-80. A set of dynamic field tests were conducted on the AZMB in November 2003, just before the bridge opening to traffic. These tests provided a unique opportunity to identify the modal properties of the bridge in its as-built condition with no previous traffic loads or seismic excitation. A benchmark study on modal identification of the AZMB is performed using three different state-of-the-art system identification algorithms based on ambient, as well as forced vibration measurements. These system identification methods consist of: (1) the multiple-reference natural excitation technique combined with the eigensystem realization algorithm; (2) the data-driven stochastic subspace identification method; and (3) the enhanced frequency domain decomposition method. Overall, the modal parameters identified using these system identification methods are found to be in very good agreement for each type of tests (ambient and forced vibration tests). For most vibration modes, the natural frequencies and mode shapes identified using the two different types of test data also match very well. However, the modal damping ratios identified from forced vibration test data are, in general, higher than those estimated from ambient vibration data. The identified natural frequencies and mode shapes are finally compared with their analytical counterparts from a three-dimensional finite-element model of the AZMB. The modal properties of the AZMB presented in this paper can be used as baseline in future health monitoring studies of this bridge.

**DOI:** 10.1061/(ASCE)0733-9445(2009)135:1(54)

**CE Database subject headings:** Bridges; California; San Francisco; Field tests; Excitation; Stochastic processes.

## Introduction

Experimental modal analysis has been widely used in the civil engineering research community to extract structural modal parameters (e.g., natural frequencies, damping ratios, and mode shapes) from vibration measurements. In classical experimental modal analysis, the frequency response functions (FRFs) in the frequency domain or impulse response functions (IRFs) in the time domain are usually the basis of system identification algorithms, which produce accurate estimates of modal parameters provided that the signal-to-noise ratio of the dynamic measurement data is high enough. However, it is very difficult to obtain FRFs or IRFs in dynamic field tests of civil structures, as typically only the structure dynamic response (output) can be measured in such tests. Especially in the case of large and flexible bridges (such as suspension and cable-stayed bridges) with natural frequencies of the predominant vibration modes in the range 0–1 Hz, it is extremely challenging and costly to provide controlled excitation for significant level of response. Thus, system identification methods based on response-only measurements (output only) have received increasing attention and have been applied successfully in the civil engineering community in recent years.

Output-only system identification methods can be classified into two main groups, namely (1) frequency domain methods and (2) time domain methods. The major frequency domain methods, such as the peak picking method, the frequency domain decomposition technique (Brincker et al. 2000) and the enhanced FDD (EFDD) technique (Brincker et al. 2001), are developed based on response auto/cross-spectral densities. Time domain output-only system identification methods can be subdivided into two categories, namely (1) two-stage methods and (2) one-stage methods. In the two-stage approaches, free vibration response estimates, including random decrement functions and response correlation functions, are obtained in the first stage from response measurements, and then modal parameters are identified in the second stage using any classical system identification algorithm based on impulse/free response function estimates. These classical system identification algorithms include the Ibrahim time domain method (Ibrahim and Mikulcik 1977), the multiple-reference Ibrahim time domain method (Fukuzono 1986), the least-squares complex exponential method (Brown et al. 1979), the polyreference complex exponential method (Vold et al. 1982), and the eigensystem real-

[1]Assistant Bridge Engineer, AECOM Transportation, 999 Town & Country Rd., Orange, CA 92868. E-mail: daniel.he@aecom.com

[2]Assistant Professor, Dept. of Civil and Environmental Engineering, Tufts Univ., 200 College Ave., Medford, MA 02155. E-mail: babak.moaveni@tufts.edu

[3]Professor, Dept. of Structural Engineering, Univ. of California at San Diego, 9500 Gilman Dr., La Jolla, CA 92093-0085 (corresponding author). E-mail: jpconte@ucsd.edu

[4]Professor, Dept. of Structural Engineering, Univ. of California at San Diego, 9500 Gilman Dr., La Jolla, CA 92093-0085. E-mail: elgamal@ucsd.edu

[5]Professor, Dept. of Civil and Environmental Engineering, Univ. of Southern California, 3620 South Vermont, Los Angeles, CA 90089-2531. E-mail: masri@usc.edu

Note. Associate Editor: Ahmet Emin Aktan. Discussion open until June 1, 2009. Separate discussions must be submitted for individual papers. The manuscript for this paper was submitted for review and possible publication on July 2, 2007; approved on July 1, 2008. This paper is part of the ***Journal of Structural Engineering***, Vol. 135, No. 1, January 1, 2009. ©ASCE, ISSN 0733-9445/2009/1-54–66/$25.00.

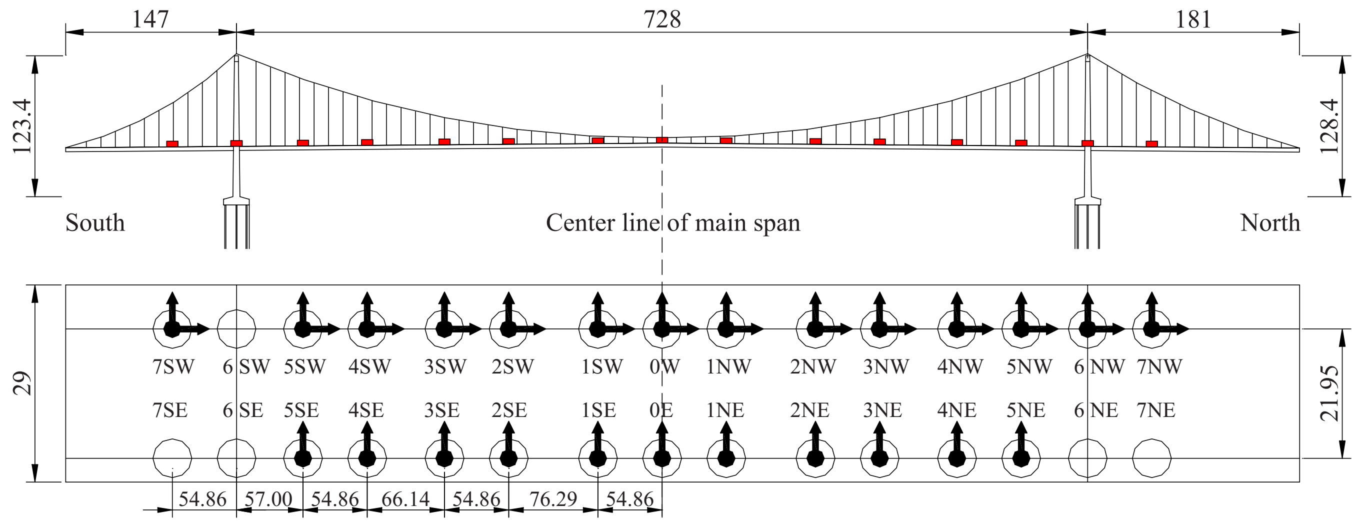


**Fig. 1.** Overall dimensions of the AZMB and instrumentation (accelerometers) layout (m)

ization algorithm (ERA) (Juang and Pappa 1985). In contrast to two-stage approaches, one-stage system identification methods such as the data-driven stochastic subspace identification (SSI-DATA) method (Van Overschee and De Moor 1996) can be used to identify modal parameters based on output-only measurements directly.

In this study, three different output-only system identification algorithms were applied to dynamic field test data collected from the Alfred Zampa Memorial Bridge (AZMB), a newly built long-span suspension bridge in California. These methods consist of: (1) the multiple-reference natural excitation technique (James et al. 1993) combined with ERA (MNExT-ERA), a two-stage time-domain system identification method; (2) SSI-DATA, a one-stage time-domain system identification method; and (3) EFDD, a nonparametric frequency domain system identification method, which is a sophisticated extension of the well-known peak picking technique. Different system identification methods provide modal parameter estimators with different intramethod and inter-method statistical properties (bias, variance, covariance), which depend on the amplitude and frequency content of the input excitation, the degree of violation of the assumed amplitude stationarity, etc. Recently, the writers have investigated the effects of such factors on the performance of the three system identification methods used in this study, based on the dynamic response of a structure (seven-story reinforced concrete building) simulated using a three-dimensional nonlinear finite-element (FE) model (Moaveni et al. 2007). It was found that for all three methods, the estimation bias and variability for the natural frequencies and mode shapes are very small and the estimation uncertainty of the damping ratios is significantly higher than that of the natural frequencies and mode shapes. It was also found that the EFDD method tends to underestimate the damping ratios of modes with relatively low contribution. In this paper, the modal parameters of the AZMB identified using different methods and data from different types of tests are compared for cross-validation purposes and also to investigate the performance of these output-only system identification methods applied to real bridge vibration data corresponding to different excitation sources. Finally, the identified natural frequencies and mode shapes are compared with their analytical counterparts obtained from a three-dimensional (3D) FE model used in the design phase of the AZMB.

## Alfred Zampa Memorial Bridge

The Carquinez Strait, located about 32 km northeast of San Francisco, carries the Sacramento River into San Francisco Bay. Before construction of the AZMB, the strait was spanned by two steel truss bridges built in 1927 and 1958, respectively, which provide a vital link on the interstate Highway I-80 corridor. The AZMB is the third bridge crossing the Carquinez Strait and it will replace the original bridge built in 1927. With a main span of 728 m and side spans of 147 and 181 m, the AZMB is the first major suspension bridge built in the United States since the 1960s. Fig. 1 shows the overall dimensions of the bridge. The design and construction of the AZMB incorporates several innovative features that have not been used previously for a suspension bridge in the United States, namely (1) orthotropic (aerodynamic) steel deck; (2) reinforced concrete towers; and (3) large-diameter drilled shaft foundations. The AZMB is also the first suspension bridge worldwide with concrete towers in a high seismic zone.

A set of dynamic field tests were performed on the AZMB in November 2003, just prior to its opening to traffic. These tests included ambient vibration tests (mainly wind induced) and forced vibration tests based on controlled traffic loads and vehicle-induced impact loads. The controlled traffic loads consisted of two heavy trucks (about 400 kN each) traversing the bridge in well-defined relative positions and at specified velocities, whereas the impact loads were generated using one or both trucks driving over triangular-shaped steel ramps (60 cm long and 10 cm high) designed and constructed specifically for these tests. Four traffic load patterns and seven vehicle-induced impact loads configurations were used in the forced vibration tests. The vibration response of the bridge was measured through an array of 34 EpiSensors ES-U (uniaxial) and 10 EpiSensor ES-T (triaxial) force-balanced accelerometers from Kinemetrics Inc. (Pasadena, CA) installed at selected locations (stations) along both sides of the bridge deck covering the entire length of the bridge (Fig. 1). Along the west side of the bridge deck, 14 stations were instrumented with either a single EpiSensor ES-T or three EpiSensors ES-U at each station to measure the vertical, transversal and longitudinal motion components. The east side of the bridge deck was instrumented with 22 EpiSensors ES-U at 11 stations (i.e., two uniaxial accelerometers per station) measuring the vertical and transversal motion components. Instead of roving accelerometers around to the different measurement stations with fixed accelerometers at one or more reference stations (as commonly done for dynamic testing of bridges), a total of 64 channels of acceleration response data were recorded simultaneously in the tests described previously, consisting of 25 vertical, 25 horizontal, and 14 longitudinal motion components. These dynamic field tests provided a unique opportunity to determine the dynamic properties of the AZMB in its as-built (baseline) condition with no previous traffic loads or seismic excitation. More details about the bridge and the dynamic tests performed can be found elsewhere (Conte et al. 2008).

## Brief Review of System Identification Methods Used

### *Eigensystem Realization Algorithm*

The ERA was developed by Juang and Pappa (1985) for modal parameter identification and model reduction of linear systems. The discrete-time state-space representation of a finite-dimensional, linear time invariant system of order $n$ is given by

$$\mathbf{z}(k+1) = \mathbf{A}\mathbf{z}(k) + \mathbf{B}\mathbf{u}(k) \tag{1a}$$

$$\mathbf{x}(k) = \mathbf{C}\mathbf{z}(k) + \mathbf{D}\mathbf{u}(k) \tag{1b}$$

where $\mathbf{A} \in \mathbb{R}^{n\times n}, \mathbf{B} \in \mathbb{R}^{n\times l}, \mathbf{C} \in \mathbb{R}^{m\times n}, \mathbf{D} \in \mathbb{R}^{m\times l}$=state-space matrices in discrete form; $\mathbf{z}(k) \in \mathbb{R}^{n}$=state vector; $\mathbf{u}(k) \in \mathbb{R}^{l}$=load vector (vector of loading functions); and $\mathbf{x}(k) \in \mathbb{R}^{m}$ $=[x_1(k)\ x_2(k)\ \cdots\ x_m(k)]^T$, a column vector of size $m$ (=number of measured/output channels) which represents the system response at discrete time $t=k(\Delta t)$ along the $m$ measured degrees of freedom (DOFs). Free vibration response [i.e., $\mathbf{u}(k)=0$] of the system can be obtained as

$$\mathbf{x}(0) = \mathbf{C}\mathbf{z}(0); \quad \mathbf{x}(1) = \mathbf{C}\mathbf{A}\mathbf{z}(0); \quad \mathbf{x}(2) = \mathbf{C}\mathbf{A}^2\mathbf{z}(0); \ \cdots \quad \mathbf{x}(k) = \mathbf{C}\mathbf{A}^k\mathbf{z}(0) \tag{2}$$

Based on the free vibration response vector, the following $(m \times s)\times s$ Hankel matrix is formed

$$\mathbf{H}^s(k-1) = \begin{bmatrix} \mathbf{x}(k) & \mathbf{x}(k+1) & \cdots & \mathbf{x}(k+s-1) \\ \mathbf{x}(k+1) & \mathbf{x}(k+2) & \cdots & \mathbf{x}(k+s) \\ \vdots & \vdots & \ddots & \vdots \\ \mathbf{x}(k+s-1) & \mathbf{x}(k+s) & \cdots & \mathbf{x}(k+2(s-1)) \end{bmatrix}_{(m\times s)\times s} \tag{3}$$

where $s$=integer that determines the size of the Hankel matrix. A singular value decomposition of Hankel matrix $\mathbf{H}^s(0)$ is performed as

$$\mathbf{H}^s(0) = \mathbf{U}\boldsymbol{\Sigma}\mathbf{V}^T = [\mathbf{U}_n \quad \mathbf{U}_p]\begin{bmatrix} \boldsymbol{\Sigma}_n & \mathbf{0} \\ \mathbf{0} & \boldsymbol{\Sigma}_p \end{bmatrix}\begin{bmatrix} \mathbf{V}_n^T \\ \mathbf{V}_p^T \end{bmatrix} \tag{4}$$

The singular value decomposition is partitioned according to the selected number $n$ of largest singular values as shown in the above-mentioned equation in which the diagonal matrix $\boldsymbol{\Sigma}$ is split up into two diagonal submatrices: $\boldsymbol{\Sigma}_n$ and $\boldsymbol{\Sigma}_p$, which contain the $n$ largest singular values (corresponding to the order of the realized system) and remaining $p$ smallest singular values (corresponding to computational errors or noise), respectively. Then, state-space matrices $\mathbf{A}$ and $\mathbf{C}$ can be estimated as

$$\mathbf{A} = \boldsymbol{\Sigma}_n^{-1/2}\mathbf{U}_n^T\mathbf{H}^s(1)\mathbf{V}_n\boldsymbol{\Sigma}_n^{-1/2} \tag{5a}$$

$$\mathbf{C} = \mathbf{E}_m^T\mathbf{U}_n\boldsymbol{\Sigma}_n^{1/2} \tag{5b}$$

in which $\mathbf{E}_m^T=[\mathbf{I}_m\ \mathbf{0}]$ and $\mathbf{I}_m=m\times m$ unit matrix. Based on matrices $\mathbf{A}$ and $\mathbf{C}$, the modal parameters (natural frequencies and damping ratios) of $N=n/2$ vibration modes can be obtained as

$$\omega_i = |\ln(\lambda_{2i-1})/\Delta t| \tag{6a}$$

$$\xi_i = -\cos(\text{angle}(\ln(\lambda_{2i-1}))), \quad i=1,2,\ldots,N \tag{6b}$$

where $\lambda_i$=$i$th eigenvalue of matrix $\mathbf{A}$ and $\Delta t$=sampling time. It should be noted that $\lambda_{2i-1}$ and $\lambda_{2i}$ $(i=1,2,\ldots,N)$ are complex conjugate pairs of eigenvalues, each pair corresponding to a vibration mode, i.e., the natural frequency and damping ratio obtained from $\lambda_{2i-1}$ are the same as those obtained from $\lambda_{2i}$. The vibration mode shapes are obtained as

$$\phi_i = \mathbf{C}\cdot\mathbf{T}_{2i-1} \tag{7}$$

where $\mathbf{T}_i$ denotes the $i$th eigenvector of matrix $\mathbf{A}$. Similarly, $\mathbf{T}_{2i-1}$ and $\mathbf{T}_{2i}$, $(i=1,2,\ldots,N)$, are complex conjugate pairs of eigenvectors, each pair corresponding to a vibration mode.

### *Natural Excitation Technique Combined with ERA*

The basic principle behind the natural excitation technique is that the theoretical cross-correlation function of the response processes along two different DOFs of an ambient (broadband) excited structure has the same analytical form as the impulse response function (or, more generally, the free vibration response) of the structure (James et al. 1993; Farrar and James 1997; Caicedo et al. 2004). Once an estimation of the cross-correlation vector is obtained for a given reference channel, the ERA method reviewed earlier can be used to estimate the modal parameters.

In order to improve the reliability and accuracy of the identified modal parameters, the multiple-reference NExT-ERA (MNExT-ERA) method (He et al. 2006) was applied as an extension of NExT-ERA. The issue of multiple reference was also discussed extensively and applied by Peeters and De Roeck (1999) in the context of the covariance-driven stochastic subspace identification method. In MNExT-ERA, instead of using a single (scalar) reference response channel as in NExT-ERA, a vector of reference channels (multiple-reference channels) is used to obtain an output cross-correlation matrix. The correlation matrix between an $N$-DOF response vector $\mathbf{X}(t)$ (e.g., nodal displacements, velocities, or accelerations) and a subset of this response vector, $\mathbf{X}^r(t)$ (with $N_r$ reference channels), is defined as

$$\mathbf{R}_{\mathbf{X}^r\mathbf{X}}(\tau) = [\mathbf{R}_{X_1^r\mathbf{X}}(\tau) \quad \mathbf{R}_{X_2^r\mathbf{X}}(\tau) \quad \cdots \quad \mathbf{R}_{X_{N_r}^r\mathbf{X}}(\tau)]_{N\times N_r} \tag{8}$$

It can be seen that each column of the cross-correlation matrix $\mathbf{R}_{\mathbf{X}^r\mathbf{X}}(\tau)$=cross-correlation vector between the system response vector and a single (scalar) reference response. The cross-correlation matrix $\mathbf{R}_{\mathbf{X}^r\mathbf{X}}(\tau)$ is then used to form Hankel matrices for application of ERA and identifying modal parameters. The basic idea behind the use of multiple reference channels (as opposed to the classical approach of using a single reference channel) is to avoid missing modes in the NExT-ERA identification process due to the proximity of the reference channel to nodes of these modes. In the case that a single cross-correlation vector does not contain significant information about a given vibration mode, the latter can still be identified accurately in MNExT-ERA through output cross-correlation functions based on other reference channels. In MNExT-ERA, the ERA is applied in its multiple-input, multiple-output formulation, but instead of forming the Hankel matrix based on the free vibration response of a truly multiple-input system, the block Hankel matrix is formed by including $N_r$ cross-correlation vectors with different reference channels.

### Data-Driven Stochastic Subspace Identification

The stochastic discrete-time state-space representation of a finite-dimensional, linear time invariant system of order $n$ can be extended from Eq. (1) to

$$\mathbf{z}(k+1) = \mathbf{A}\mathbf{z}(k) + \mathbf{w}(k) \tag{9a}$$

$$\mathbf{x}(k) = \mathbf{C}\mathbf{z}(k) + \mathbf{v}(k) \tag{9b}$$

where state-space matrices $\mathbf{A}$ and $\mathbf{C}$=same as in Eq. (1): $\mathbf{A}$=state transition matrix, which completely characterizes the dynamics of the system through its eigenproperties, and $\mathbf{C}$=output matrix that specifies how the inner states are transformed into the measured system response/output; $\mathbf{w}(k) \in \mathbb{R}^n$=process noise due to external disturbances and modeling inaccuracies (i.e., missing high-frequency dynamics); and $\mathbf{v}(k) \in \mathbb{R}^m$=measurement noise due to sensor inaccuracies. As the input $\mathbf{u}(k)$, see Eq. (1), is unknown and it is impossible to distinguish the input information from the noise terms $\mathbf{w}(k)$ and $\mathbf{v}(k)$, the input is implicitly included in these noise terms. Both noise terms $\mathbf{w}(k)$ and $\mathbf{v}(k)$ are assumed to be zero mean, white vector sequences. Data-driven stochastic subspace identification (SSI-DATA) is a method to estimate state-space matrices $\mathbf{A}$ and $\mathbf{C}$ using output-only measurements directly. Compared to two-stage time-domain system identification methods such as NExT-ERA, SSI-DATA does not require any preprocessing of the data to calculate auto/cross-correlation functions or auto/cross-spectra of output data. In addition, robust numerical techniques such as QR factorization (i.e., orthogonal-triangular decomposition) singular value decomposition (SVD) and least squares are involved in this method. The procedure of extracting the state-space matrices $\mathbf{A}$ and $\mathbf{C}$ can be summarized as follows: (1) form the output Hankel matrix and partition it into "past" and "future" output submatrices; (2) calculate the orthogonal projection of the row space of the future output sub-matrix into the row space of the past output submatrix using QR factorization; (3) obtain the observability matrix and Kalman filter state estimate via SVD of the projection matrix; and (4) using the available Kalman filter state estimate, extract the discrete-time system state-space matrices based on a least-squares solution. Once the system state-space matrices are determined, the modal parameters can be obtained by using Eqs. (6) and (7). More details about stochastic subspace identification can be found in Van Overschee and De Moor (1996).

### Enhanced Frequency Domain Decomposition

The FDD method, a nonparametric frequency-domain approach, is an extension of the basic frequency domain approach referred to as peak picking technique. According to the FDD technique, the modal parameters are estimated through SVD of the power spectral density (PSD) matrix performed at all discrete frequencies. Considering a lightly damped system, the number of vibration modes contributing significantly to a given cross-spectral density (CSD) function at a particular frequency is limited to a small number (usually 1 or 2). Through the above-mentioned SVD, CSD functions are decomposed into single-degree-of-freedom (SDOF) CSD functions, each corresponding to a single vibration mode of the dynamic system. In the EFDD method (Brincker et al. 2001), the natural frequency and damping ratio of a vibration mode are identified from the SDOF CSD function corresponding to that mode. For this purpose, the SDOF CSD function is taken back to the time domain by inverse Fourier transformation, and the frequency and damping ratio of the mode considered are estimated from the zero-crossing times and the logarithmic decrement, respectively, of the corresponding SDOF autocorrelation function.

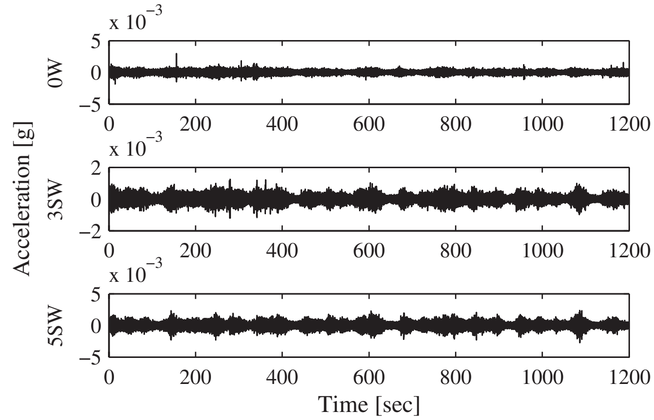


**Fig. 2.** Vertical acceleration response measured during the ambient vibration test

## System Identification Results

System identification of the AZMB was performed based on both ambient and forced vibration test data. During the dynamic tests, the bridge acceleration response at various points (stations) was sampled at a rate of 200 Hz resulting in a Nyquist frequency of 100 Hz, which is much higher than the frequencies of interest in this study (<4 Hz). The 20 min long ambient vibration test data used in this study were collected just after midnight local time, whereas there were no construction activities on the bridge. Therefore, the bridge ambient vibrations were driven mainly by wind [Test No. 18 (Conte et al. 2008)]. Fig. 2 shows the bridge vertical acceleration response at the midpoint, south quarter point and near the south end of the main span on the west side of the bridge deck (i.e., Stations 0W, 3SW, and 5SW, respectively) measured during the ambient vibration test. The Fourier amplitude spectrum of the vertical acceleration response measured at Station 3SW is shown in Fig. 3. For long-span suspension bridges such as the AZMB, the natural frequencies of the lower (and predominant) vibration modes lie in the range 0–1 Hz. However, from Fourier amplitude spectra of the measured acceleration responses, it was observed that vibration modes with natural frequencies in the range 1–4 Hz were also significantly excited in the ambient vibration test. The vibration modes above 1 Hz were excited as much as those below 1 Hz. Despite the fact that the amplitude of the measured ambient vibration response is much lower than that of the forced vibration response (see Fig. 4), the ambient vibration data was found to be very clean (i.e., high signal-to-noise ratio) especially for identifying the lower vibration modes (with natural frequencies below 1 Hz).

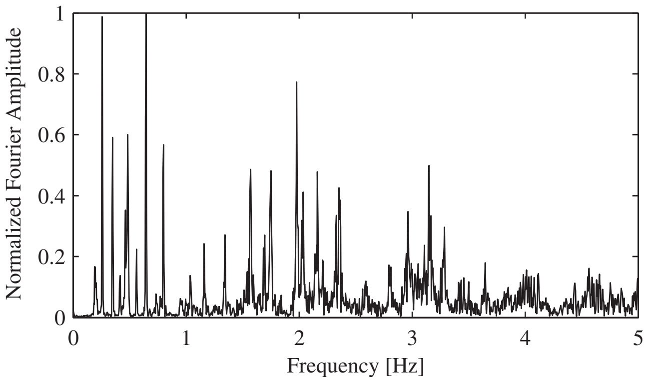


**Fig. 3.** Fourier amplitude spectrum of vertical acceleration response at Station 3SW measured during the ambient vibration test

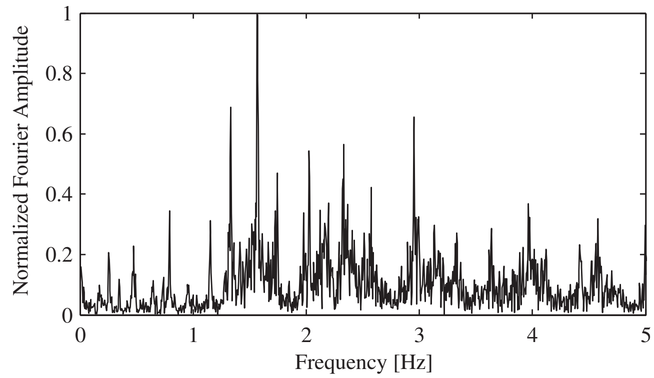


**Fig. 5.** Fourier amplitude spectrum of vertical acceleration response at Station 3SW measured during the six controlled traffic load tests

As described in the previous section, two types of forced vibration tests were performed on the AZMB, namely (1) controlled traffic load tests and (2) vehicle-induced impact tests. In the vehicle-induced impact tests, the load applied to the bridge departed from an ideal impulse load due to the continuous motion of the truck on the bridge before and after the impact, which causes errors in identifying the damping ratios (He et al. 2006). Therefore, the bridge vibration data from the vehicle-induced impact tests were not used to identify the bridge modal parameters in this study. Although the AZMB has a total of four traffic lanes, the trucks could only use the two middle lanes during the tests. Six different controlled traffic load tests were performed: (1) both trucks crossing over the bridge in parallel at the velocity of 48 km/h; (2) one truck crossing over the bridge at the velocity of 48 km/h; (3) both trucks crossing over the bridge in opposite directions at the velocity of 48 km/h; (4) both trucks crossing over the bridge in opposite directions at the velocity of 24 km/h; (5) one truck crossing over the bridge at the velocity of 24 km/h; and (6) both trucks crossing over the bridge in parallel at the velocity of 24 km/h (Conte et al. 2008). Due to the limited duration of each test (100 s for Tests No. 1, 2, and 3 and 200 seconds for Tests No. 4, 5, and 6) and the requirement of high frequency resolution (to resolve closely spaced vibration modes) in the system identification, the bridge vibration measurements from the six different tests are concatenated back to back resulting in a total duration of 900 s (15 min). As an illustration, Fig. 4 shows the bridge vertical acceleration response at the midpoint, south quarter point and near the south end of main span on the west side of the bridge deck (i.e., Stations 0W, 3SW, and 5SW, respectively) measured during the six forced vibration tests. The amplitude of vibration of the bridge during the first 300 s (trucks moving at 48 km/h) is larger than during the last 600 s (trucks moving at 24 km/h). By comparing Fig. 2 and Fig. 4, it is observed that the amplitude of the bridge vibration in the forced vibration tests is approximately one order of magnitude larger than that in the ambient vibration test. The Fourier amplitude spectrum of the vertical acceleration response measured at Station 3SW during the six forced vibration tests is shown in Fig. 5. It is observed that during the controlled traffic load tests, the vibration modes with natural frequency above 1 Hz (higher vibration modes) are more significantly excited than those with natural frequency below 1 Hz (lower vibration modes), which renders the latter more difficult to identify.

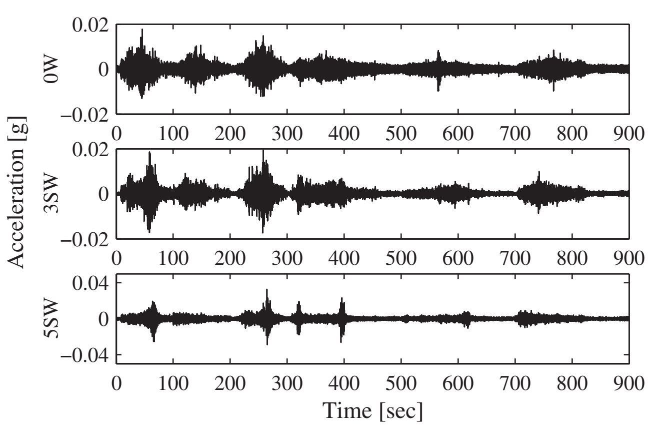


**Fig. 4.** Vertical acceleration response measured during the six controlled traffic load tests

In this study, both lower vibration modes (with natural frequency below 1 Hz) and higher vibration modes (with natural frequency in the range 1–4 Hz) were identified. However, if all the vibration modes in the frequency range 0–4 Hz are considered in a single identification for each set of measurement data (i.e., ambient or forced vibration data), then based on the stabilization diagram a very high model order must be selected to avoid missing any of the vibration modes of interest. Selection of a high order for the realized model leads to a large number of mathematical (nonphysical) modes, which will obstruct the identification of the true physical vibration modes of the bridge. Thus, in order to improve the computational efficiency and avoid missing modes in the system identification process, the lower vibration modes (with natural frequencies below 1 Hz) and higher vibration modes (with natural frequencies above 1 Hz) are identified separately by applying to the bridge vibration data a low-pass Butterworth infinite impulse response filter of order 7 with a cut-off frequency of 1 Hz and a band-pass finite impulse response filter of order 1,024 with lower and upper cut-off frequencies of 1 and 4 Hz, respectively. Only vertical response measurements were used to identify the higher vibration modes.

### System Identification Results Based on Ambient Vibration Data

In the implementation of MNExT-ERA, Stations 1NE, 2SW, 3NW, and 4SE were used as reference stations and response correlation functions were estimated through inverse Fourier transformation of the corresponding PSD functions. Estimation of the PSD functions was based on Welch-Bartlett method using 300 s

**Table 1.** System Identification Results Based on the Ambient Vibration Data

| | Natural frequencies (Hz) | | | Damping ratios (%) | | | MAC values | | |
|---|---|---|---|---|---|---|---|---|---|
| Modes | MNEXT-ERA | SSI-DATA | EFDD | MNEXT-ERA | SSI-DATA | EFDD | MNExT and SSI | MNExT and EFDD | SSI and EFDD |
| 1-S-H | 0.159 | 0.158 | 0.161 | 1.29 | 0.50 | 2.47 | 1.000 | 1.000 | 1.000 |
| 1-S-V | 0.194 | 0.193 | 0.193 | 0.27 | 0.21 | 0.89 | 0.998 | 1.000 | 0.997 |
| 1-AS-V | 0.204 | 0.201 | | 1.98 | 1.36 | | 0.991 | | |
| 2-S-V | 0.258 | 0.258 | 0.259 | 0.21 | 0.23 | 1.00 | 1.000 | 1.000 | 1.000 |
| 2-AS-V | 0.350 | 0.350 | 0.349 | 0.15 | 0.20 | 0.66 | 1.000 | 1.000 | 1.000 |
| 1-AS-H | 0.361 | 0.365 | 0.361 | 1.68 | 0.49 | 0.92 | 0.985 | 0.987 | 0.998 |
| | 0.414 | 0.414 | 0.415 | 0.23 | 0.13 | 0.72 | 1.000 | 1.000 | 1.000 |
| 1-S-T | 0.469 | 0.471 | 0.476 | 1.29 | 0.17 | 0.48 | 0.976 | 0.994 | 0.991 |
| 3-S-V | 0.484 | 0.483 | 0.484 | 0.15 | 0.21 | 0.71 | 0.996 | 0.997 | 0.999 |
| | 0.561 | 0.561 | 0.562 | 0.16 | 0.15 | 0.34 | 0.997 | 1.000 | 0.996 |
| 3-AS-V | 0.645 | 0.645 | 0.645 | 0.09 | 0.11 | 0.42 | 1.000 | 1.000 | 1.000 |
| 1-AS-T | 0.738 | 0.741 | 0.737 | 0.18 | 0.34 | 0.28 | 0.986 | 0.995 | 0.995 |
| 4-S-V | 0.799 | 0.799 | 0.799 | 0.16 | 0.23 | 0.34 | 0.998 | 0.999 | 1.000 |
| 4-AS-V | 0.958 | 0.956 | 0.957 | 0.27 | 0.15 | 0.17 | 0.994 | 0.973 | 0.986 |
| 2-S-T | 1.003 | 1.007 | | 2.97 | 0.58 | | 0.980 | | |
| 4-AS-V | 1.036 | 1.035 | 1.038 | 0.11 | 0.22 | 0.24 | 0.994 | 0.997 | 0.987 |
| 5-S-V | 1.160 | 1.174 | 1.165 | 0.18 | 0.36 | 0.50 | 0.991 | 1.000 | 0.992 |
| 5-AS-V | 1.345 | | 1.343 | 0.46 | | 0.11 | | 0.950 | |
| 2-AS-T | 1.367 | 1.360 | 1.362 | 1.00 | 0.26 | 0.19 | 0.934 | 0.806 | 0.875 |
| 6-S-V | 1.572 | 1.575 | 1.570 | 0.63 | 0.30 | 0.14 | 0.988 | 0.997 | 0.994 |
| 3-S-T | 1.684 | 1.689 | 1.685 | 0.17 | 0.09 | 0.26 | 0.988 | 0.998 | 0.992 |
| 3-AS-T | 2.029 | 2.025 | 2.034 | 0.34 | 0.13 | 0.14 | 0.647 | 0.940 | 0.781 |
| 4-S-T | 2.331 | 2.340 | | 0.21 | 0.32 | | 0.318 | | |
| 4-AS-T | 2.671 | 2.673 | 2.676 | 0.40 | 0.45 | 0.00 | 0.673 | 0.881 | 0.740 |
| 5-S-T | 2.949 | 2.948 | 2.947 | 0.27 | 0.13 | 0.08 | 0.682 | 0.996 | 0.706 |
| 5-AS-T | 3.273 | 3.271 | 3.301 | 0.59 | 0.15 | 0.00 | 0.910 | 0.420 | 0.363 |

Note: In the first column, S=symmetric; AS=antisymmetric; H, V, T=horizontal, vertical, and torsional modes, respectively. An empty cell in the first column indicates that the corresponding mode is neither a symmetric nor an antisymmetric mode. An empty cell in the second through sixth columns indicates that the natural frequency and/or damping ratio is not available because the corresponding vibration mode was missed in the identification process.

long (60,000 points) Hanning windows with 50% overlap, in order to reduce the effects of spectral leakage. In order to increase the computational efficiency of the system identification procedure, the estimated auto/cross-correlation functions were down sampled to 10 and 40 Hz for identifying lower and higher vibration modes, respectively. After down sampling, the Nyquist frequency is still much higher than the frequency range of interest ($\leq 1$ Hz for lower vibration modes and $\leq 4$ Hz for higher vibration modes). The down-sampled estimated auto/cross-correlation functions were then used to form Hankel matrices for applying ERA in the second stage of the modal identification. Due to the fact that the accelerometer measuring the vertical response at Station 5SE was not functioning properly, the Hankel matrix constructed using vertical vibration data for identifying lower vibration modes has dimensions $(21\times 200)\times(4\times 200)$ (21 stations, 4 reference stations), whereas the Hankel matrix based on horizontal vibration data has dimensions $(22\times 200)\times(4\times 200)$ (22 stations). For identifying the higher vibration modes, a Hankel matrix of dimensions $(21\times 400)\times(4\times 400)$ was constructed. The natural frequencies and damping ratios of the identified vibration modes are reported in Table 1 together with those identified using the two other methods. It should be noted that the modal parameters of some significant higher vertical vibration modes (beyond the sixth symmetric and antisymmetric vertical modes) are not reported here, because the corresponding mode shapes could not be classified/recognized due to insufficient spatial density of the sensor network deployed along the bridge deck.

In applying SSI-DATA to identify the modal parameters of the lower vibration modes, the filtered measured data were first down sampled to 10 Hz and then used to form the output Hankel matrix composed of 100 block rows with either 21 rows in each block (21 vertical channels) for identifying vertical modes or 22 rows in each block (22 horizontal channels) for identifying horizontal modes. In identifying the higher vibration modes using SSI-DATA, the filtered measured data were first down sampled to 40 Hz and then used to form the output Hankel matrix composed of 50 block rows with 21 rows in each block (21 vertical channels). The identified natural frequencies and damping ratios are reported in Table 1. In the application of MNExT-ERA and SSI-DATA in this study, a stabilization diagram was used to determine the "optimum" order of the realized system from which the modal parameters are extracted. For example, in identifying the modal parameters of the lower vibration modes (below 1 Hz) using SSI-DATA based on the ambient vibration data, the order of the realized system was determined as $n=32$.

In the implementation of EFDD, the 20 min long filtered ambient vibration data were also down sampled to 10 and 40 Hz for identifying lower and higher vibration modes, respectively. Estimation of the PSD functions was based on the Welch–Bartlett method using 300 s long Hanning windows with 50% overlap.

The modal frequencies were estimated at peak locations (i.e., peak picking) in the first singular value versus frequency plot and the mode shapes were estimated by the first singular vector at the corresponding frequencies (Brincker et al. 2001). The SDOF CSD functions are estimated from the first singular value plot using a modal assurance criterion (MAC) (Allemang and Brown 1982) higher than 0.95 between the estimated mode shape and the singular vectors at discrete frequencies around the natural frequency. The modal parameters estimated using EFDD are given in Table 1.

From Table 1, it is observed that the natural frequencies identified using the three system identification methods considered here are in excellent agreement, except for a few modes, which could not be identified by all three methods, such as the first antisymmetric vertical mode (1-AS-V) missed using EFDD and the 5-AS-V mode missed by the SSI-DATA method. The fact that certain modes (1-AS-V, 2-S-T, 5-AS-V, 4-S-T) could not be identified by all three methods is likely due to the low relative participation of these modes to the measured dynamic responses. It is found that the relative difference in the identified damping ratios obtained using different methods is significantly larger than that of the corresponding identified natural frequencies. This is a well-known fact widely reported in the structural identification literature, namely that the estimation uncertainty of damping ratios is inherently higher (by more than an order of magnitude for the coefficient of variation) than that of the corresponding natural frequencies. The following facts are also worth noting regarding the identification of damping ratios: (1) the estimation uncertainty of the damping ratios is generally higher for output-only than for input-output system identification methods, as the input signals do not strictly satisfy the broadband assumption behind the formulation of output-only methods. Different methods provide modal parameter estimators with different intramethod and intermethods statistical properties (bias, variance, covariance), which depend on the frequency content of the input excitation and the level of violation of the assumed amplitude stationarity; and (2) linear viscous damping is assumed in the structural model underlying the system identification, which in many cases may not characterize well the actual energy dissipation mechanisms of the structure. This is a source of modeling uncertainty/error that will contribute to the uncertainty of the identified modal damping ratio. Although the damping ratio estimates provided by this study have a relatively large variability across methods (compared to natural frequencies), they are all in a reasonable range (i.e., positive and less than 3%) compared to other structural identification studies reported in the literature with double digit and/or negative damping ratios. Further, estimated damping ratios reveal more reliably/clearly imperfections in data preprocessing and parameter estimation than the estimated natural frequencies. Therefore, the reasonable estimated damping ratios obtained in this study validate/verify the extensive numerical operations involved in the advanced system identification methods used. The accuracy of the estimated damping ratios could be improved by using longer durations of response measurements (to be recorded first), and larger amplitude ambient excitation. However, the estimation uncertainty of the damping ratios will always remain above some lower bound from estimation theory (e.g., Cramer–Rao bound) and the fact that linear viscous damping is only at best a very approximate model of the dissipative forces within a structure further aggravates the situation. It is worth noting that the EFDD method provides near-zero modal damping ratios for some higher torsional modes (4-AS-T, 5-S-T, 5-AS-T) and appears to underestimate these damping ratios compared to the other two methods (see Table 1). Finally, it is worth mentioning that the identified modal damping ratios might be influenced by the aerodynamic damping induced by the wind–structure interaction.

The vibration mode shapes identified using MNExT-ERA, SSI-DATA, and EFDD are complex valued. Fig. 6 represents in polar plots (i.e., rotating vectors in the complex plane) the mode shapes of the AZMB (main span only) identified using MNExT-ERA based on ambient vibration data. These polar plots have the advantage to show directly the extent of the nonproportional damping characteristics of a vibration mode. If all complex valued components of a mode shape vector are collinear (i.e., in phase or 180° out of phase), this vibration mode is said to be classically (or proportionally) damped. On the other hand, the more these mode shape components are scattered in the complex plane, the more the vibration mode is nonclassically (or nonproportionally) damped. However, measurement noise, estimation errors, and modeling errors could also cause a "true" classically damped mode to be identified as nonclassically damped. Fig. 6 shows that most of the vibration modes identified in this study are either perfectly or nearly classically damped except for some higher vibration modes (5-AS-V, 2-AS-T, 3-AS-T, 4-S-T, 4-AS-T). A 3D representation of the normalized mode shapes for these identified vibration modes is given in Fig. 7. Normalization was performed by projecting all mode shape components onto their principal axis (in the complex plane) and then scaling this projected mode shape vector for a unit value of its largest component. The identified space-discrete mode shapes were interpolated between the sensor locations using cubic splines along both sides of the bridge deck and straight lines along the deck transverse direction. As the accelerometers at Stations 6SW, 6SE, 7SE, 6NE, and 7NE could not be recorded, the vibration mode shapes are plotted over the bridge main span only and are based on the assumption that the motion of the bridge deck at the towers is restrained in both the horizontal and vertical direction. In addition, the vertical acceleration response at Station 5SE was not recorded properly during the tests, and the mode shape components at Stations 5NE and 5SW were used to estimate the component at Station 5SE based on the symmetric or antisymmetric property of vibration modes. From Fig. 7, it is observed that: (1) the identified mode shapes with natural frequencies of 0.41 and 0.56 Hz (observed only over the main span in this study) are neither symmetric nor antisymmetric with respect to the centerline of the main span and (2) the identified modes with natural frequencies of 0.96 and 1.04 Hz have similar mode shapes (i.e., 4-AS-V). Additional measurement stations on the towers and approach spans (which have different lengths) are needed to identify the corresponding bridge global mode shapes.

MAC values were computed in order to compare corresponding mode shapes identified using different system identification methods and are reported in Table 1. The high MAC values obtained for most vibration modes indicate an excellent agreement between the mode shapes identified using different methods based on ambient vibration data. The low MAC values of higher torsional modes such as 4-S-T (i.e., fourth symmetric torsional mode) and 5-AS-T (i.e., fifth antisymmetric torsional mode) indicate that the accuracy of these identified mode shapes is not as high as that for lower vibration modes, which could be due to the low participation (relative to other modes) of these modes to the measured bridge response.

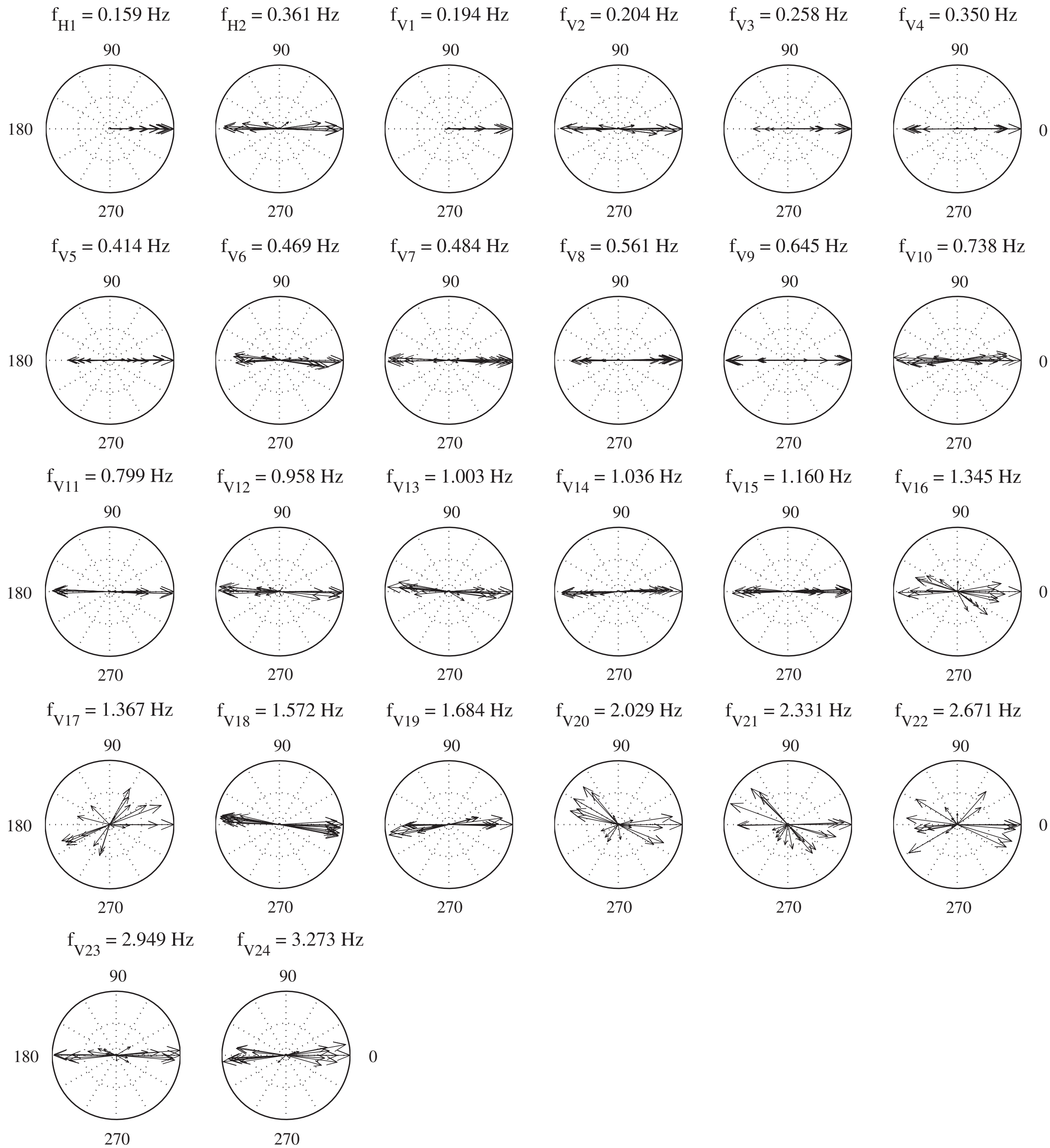


**Fig. 6.** Polar plot representation of vibration mode shapes identified using MNExT-ERA based on ambient vibration data

### *System Identification Results Based on Forced Vibration Data*

The system identification methods MNExT-ERA, SSI-DATA, and EFDD were also applied to identify the bridge modal parameters based on forced vibration test data. MNExT-ERA and EFDD were implemented in exactly the same way as for ambient vibration data. However, in applying SSI-DATA to identify the higher vibration modes, an output Hankel matrix was formed composed of 60 block rows instead of 50 (for ambient vibration data) due to the fact that the forced vibration tests are of shorter duration than the ambient vibration test. The modal parameters identified using these three methods based on the forced vibration data are reported in Table 2. The identified natural frequencies using different methods are found to be in excellent agreement. The modal damping ratios of some vibration modes such as 1-AS-V, 1-S-T, and 2-AS-T identified using EFDD are near zero. Excluding these modes, the modal damping ratios estimated using the different methods are in reasonable agreement, especially those identified

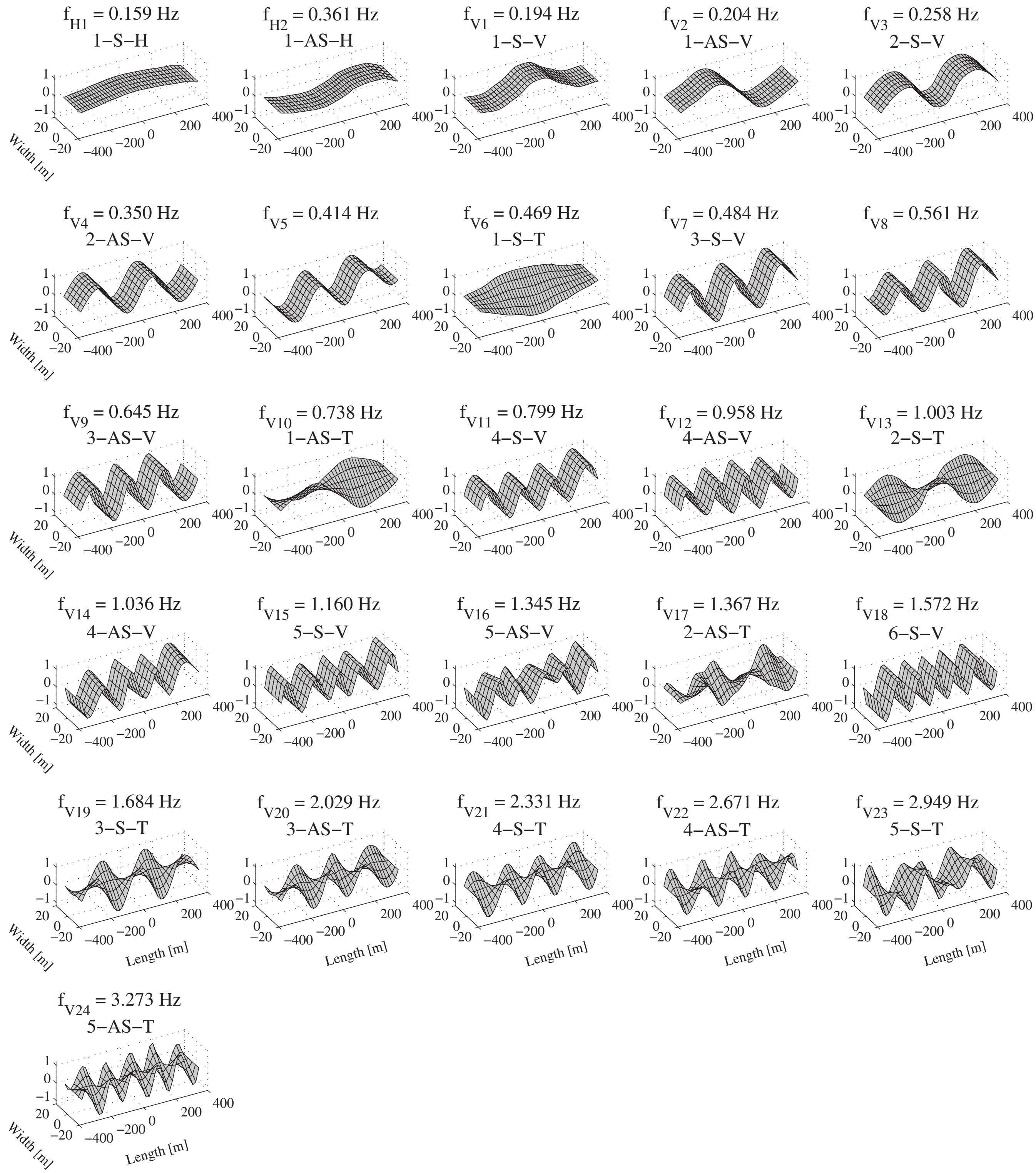


**Fig. 7.** 3D representation of normalized vibration mode shapes identified using MNExT-ERA based on ambient vibration data

using MNExT-ERA and SSI-DATA. The high MAC values obtained for most vibration modes indicate an excellent agreement between the mode shapes identified using different methods based on forced vibration test data. The low MAC values obtained for a few modes, such as the 1-AS-V and the mode with a natural frequency of 0.41 Hz, could be due to the low relative participation of these modes to the measured forced vibration response of the bridge.

By comparing the average values of the modal parameters (natural frequencies and modal damping ratios) identified using the three methods based on the ambient vibration data (see Table 1) with their counterparts identified based on the forced vibration data (see Table 2), it is found that: (1) the natural frequencies identified using the two types of test data are in excellent agreement except for the 1-AS-V mode. The significant difference in the identified natural frequencies for this mode reflects the diffi-

**Table 2.** System Identification Results Based on Forced Vibration Test Data

| | Natural frequencies (Hz) | | | Damping ratios (%) | | | MAC values | | |
|---|---|---|---|---|---|---|---|---|---|
| Modes | MNEXT-ERA | SSI-DATA | EFDD | MNEXT-ERA | SSI-DATA | EFDD | MNExT and SSI | MNExT and EFDD | SSI and EFDD |
| 1-S-H | 0.160 | 0.165 | 0.161 | 3.56 | 1.53 | 0.89 | 0.998 | 0.998 | 0.999 |
| 1-AS-V | 0.174 | 0.172 | 0.176 | 9.11 | 6.84 | 0.00 | 0.697 | 0.711 | 0.517 |
| 1-S-V | 0.194 | 0.193 | 0.195 | 1.77 | 1.23 | 0.97 | 0.961 | 0.998 | 0.966 |
| 2-S-V | 0.257 | 0.256 | 0.252 | 1.00 | 0.47 | 1.72 | 0.998 | 0.997 | 0.993 |
| 2-AS-V | 0.349 | 0.348 | 0.349 | 0.59 | 0.39 | 1.07 | 0.996 | 1.000 | 0.996 |
| 1-AS-H | 0.366 | 0.368 | 0.361 | 1.98 | 1.67 | 0.66 | 0.956 | 0.954 | 0.944 |
| | 0.407 | 0.408 | 0.405 | 2.02 | 2.52 | 0.82 | 0.842 | 0.916 | 0.788 |
| 1-S-T | 0.473 | 0.469 | 0.479 | 0.81 | 0.36 | 0.00 | 0.989 | 0.998 | 0.988 |
| 3-S-V | 0.478 | 0.484 | | 1.76 | 1.51 | | 0.902 | | |
| | 0.561 | 0.559 | 0.564 | 1.30 | 0.97 | 0.39 | 0.974 | 0.956 | 0.983 |
| 3-AS-V | 0.645 | 0.644 | 0.647 | 1.02 | 0.79 | 0.63 | 0.997 | 0.986 | 0.982 |
| 1-AS-T | 0.736 | 0.736 | 0.733 | 0.30 | 0.25 | 0.50 | 0.996 | 0.998 | 0.996 |
| 4-S-V | 0.794 | 0.795 | 0.794 | 0.36 | 0.21 | 0.53 | 0.994 | 0.997 | 0.997 |
| 4-AS-V | 0.954 | 0.953 | 0.950 | 0.33 | 0.16 | 0.44 | 0.988 | 0.987 | 0.998 |
| 2-S-T | | 0.998 | | | 0.91 | | | | |
| 4-AS-V | 1.028 | 1.034 | 1.028 | 0.48 | 0.29 | 0.15 | 0.964 | 0.974 | 0.945 |
| 5-S-V | 1.152 | 1.184 | 1.152 | 0.41 | 1.42 | 0.40 | 0.980 | 0.999 | 0.982 |
| 5-AS-V | 1.334 | 1.360 | 1.333 | 1.00 | 1.44 | 0.07 | 0.941 | 0.996 | 0.945 |
| 2-AS-T | 1.366 | | 1.367 | 0.52 | | 0.00 | | 0.664 | |
| 6-S-V | 1.563 | 1.557 | 1.567 | 0.84 | 0.44 | 0.19 | 0.998 | 0.999 | 0.998 |
| 3-S-T | 1.687 | 1.699 | 1.685 | 0.31 | 0.36 | 0.09 | 0.843 | 0.932 | 0.965 |
| 3-AS-T | 2.019 | 2.021 | 2.022 | 0.27 | 0.22 | 0.20 | 0.949 | 0.967 | 0.958 |
| 4-S-T | | 2.334 | | | 0.41 | | | | |
| 4-AS-T | 2.656 | 2.657 | 2.654 | 0.23 | 0.13 | 0.25 | 0.905 | 0.972 | 0.894 |
| 5-S-T | 2.951 | 2.943 | 2.957 | 0.11 | 0.23 | 0.11 | 0.821 | 0.853 | 0.689 |
| 5-AS-T | | 3.275 | | | 0.26 | | | | |

Note: In the first column, S=symmetric; AS=antisymmetric; H, V, T=horizontal, vertical, and torsional modes, respectively. An empty cell in the first column indicates that the corresponding mode is neither a symmetric nor an antisymmetric mode. An empty cell in the second through sixth columns indicates that the natural frequency and/or damping ratio is not available because the corresponding vibration mode was missed in the identification process.

culty in identifying it due to its very low relative contribution to the bridge vibration response in both the ambient and forced vibration tests. Thus, this mode could not be reliably identified; (2) the order (in terms of natural frequency) of vibration modes 1-S-V and 1-AS-V identified based on ambient vibration data is swapped over when these modes are identified based on forced vibration data; and (3) the identified modal damping ratios are response amplitude dependent. For most vibration modes, especially for the lower vibration modes, the modal damping ratios identified using forced vibration data are higher than those identified using ambient vibration data as clearly shown in Fig. 8. The order of the vibration modes used in Fig. 8 corresponds to the sorted natural frequencies identified based on forced vibration data. Fig. 9 shows the average (over the three methods) of the MAC values between the corresponding mode shapes identified based on ambient vibration and forced vibration data. The high average MAC values obtained for most vibration modes indicate an excellent agreement between the mode shapes identified using the two types of test data. The low average MAC values obtained for a few higher torsional modes is likely due to the large estimation errors of these modes due to their low relative contributions to the measured bridge vibration response.

## Comparison between Experimental and Analytical Modal Parameters

A 3D FE model of the AZMB developed in the structural analysis software ADINA (ADINA R&D Inc. 2002) was provided by Cal-

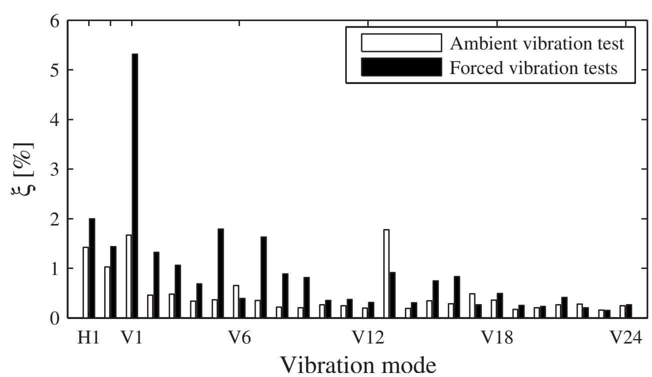


**Fig. 8.** Comparison of damping ratios identified using ambient vibration and forced vibration test data (see Fig. 6 or 7 for abbreviation of vibration modes)

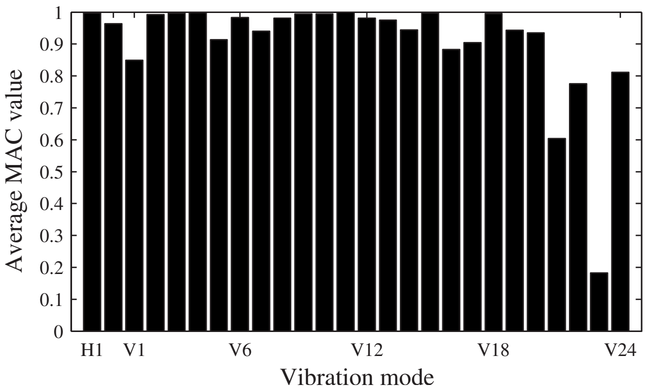


**Fig. 9.** Averaged (over the three methods) MAC values between corresponding mode shapes identified based on ambient vibration and forced vibration test data

trans (Dr. Charles Sikorsky, personal communication, 2005). This FE model is composed mainly of: (1) linear elastic frame elements (with possible initial strain) to model the two main suspension cables, suspender cables, steel box girder (in both the longitudinal and transversal directions) and tower shafts (at some specific locations, the shafts are modeled using multilinear inelastic frame elements); (2) multilinear inelastic frame elements to model the pile foundations supporting the tower shafts; and (3) linear elastic shell elements to model the pile caps. The inertia properties of the bridge are modeled with element consistent mass matrices based on element shape functions and material density. Additional lumped masses, assigned to some translational DOFs, are also included in the model to represent various equivalent masses not accounted for by the element mass matrices. This FE model of the AZMB is composed of 3,281 elements and approximately 14,000 DOFs. It was used in the design process of this bridge.

In this section, the identified natural frequencies and mode shapes of the bridge vibration modes below or slightly above 1 Hz are compared with their analytical counterparts obtained from the FE model of the bridge. The first 200 vibration modes of the FE model of the AZMB were computed. In order to pair each identified vibration mode with the corresponding analytical vibration mode, MAC values were calculated between the identified mode shape and all 200 computed mode shapes truncated at the accelerometer locations (i.e., measured DOFs) in order to have the same size as the identified mode shapes. For each identified vibration mode, the computed eigenmode with the highest MAC value was taken as its analytical counterpart. In the case where several computed eigenmodes have close high MAC values with the identified mode considered, the one with natural frequency closest to the identified natural frequency was selected. The computed natural frequencies and mode shapes corresponding to the lowest 16 identified vibration modes are shown in Fig. 10 together with the corresponding natural frequencies identified from ambient and forced vibration data, respectively, averaged over the three system identification methods used. The computed mode shapes can be directly compared to their identified counterparts in Fig. 7. By comparing the corresponding identified and analytically predicted natural frequencies (given in Fig. 10), the following observations can be made: (1) the identified and analytically predicted natural frequencies of the 1-S-V, 2-S-V, and 2-AS-V vibration modes are in excellent agreement. Their differences are less than 1%. The agreement between identified and analytical natural frequencies for the 1-AS-H, 1-S-T, and 1-AS-T modes is very good, with differences less than or slightly above 3%; (2) the discrepancies between identified and analytically predicted natural frequencies for the 1-S-H and 1-AS-V modes are significant. For the 1-S-H mode, the discrepancy is likely due to inaccuracies in the FE model, as the system identification results using different methods based on different test data are found to be in very good agreement. However, for the 1-AS-V mode, the discrepancy could be caused by both inaccuracies in the FE model and system identification errors, as the natural frequency of this mode identified using different test data are not in good agreement either; and (3) the other identified and corresponding analytically predicted natural frequencies are found to be in reasonable agreement (less than 10% difference). Fig. 11 shows in bar plot the MAC values (averaged over the three system identification methods used) between identified and analytically predicted mode shapes. For most vibration modes, there is a very good to excellent agreement between identified and analytically predicted mode shapes. The low MAC values obtained for a few modes, such as the 1-AS-V and the mode with a natural frequency of 0.41 Hz, are caused by both system identification errors due to the low relative contributions of these modes to the measured bridge vibration and inaccuracies in the FE model of the bridge.

## Summary and Conclusions

A set of dynamic field tests were conducted on the Alfred Zampa Memorial Bridge, located 32 km northeast of San Francisco on interstate Highway I-80, just before its opening to traffic in November 2003. These tests provided a unique opportunity to obtain the modal parameters of the bridge in its as-built condition with no previous traffic loads or seismic excitation.

Two time domain system identification methods, namely the multiple-reference natural excitation technique combined with the eigensystem realization algorithm (MNExT-ERA) and the data-driven stochastic subspace identification (SSI-DATA) method, as well as a frequency domain method, namely enhanced frequency domain decomposition, were applied to identify the modal parameters of the bridge based on bridge vibration data from two types of tests: ambient vibration test and forced vibration tests based on controlled-traffic loads. From the modal identification results obtained, the following conclusions can be made: (1) the natural frequencies identified using the three different methods are in excellent agreement for each type of tests; (2) the natural frequencies identified based on data from the two different types of test are also in excellent agreement, except for the 1-AS-V (first antisymmetric vertical) mode. The significant difference in the identified natural frequencies for this mode reflects the difficulty in identifying it due to its very low relative contribution to the measured bridge vibration in both the ambient and forced vibration tests. In addition, the order (in terms of natural frequency) of vibration modes 1-S-V and 1-AS-V identified based on ambient vibration data is swapped over when these modes are identified based on forced vibration data; (3) the relative difference in the identified damping ratios obtained using different methods is significantly larger than that of the corresponding identified natural frequencies. This is a well known fact widely reported in the structural identification literature, namely that the estimation uncertainty of damping ratios is inherently higher (by more than an order of magnitude for the coefficient of variation) than that of the corresponding natural frequencies; (4) for most vibration modes, especially for the lower vibration modes, the averaged modal

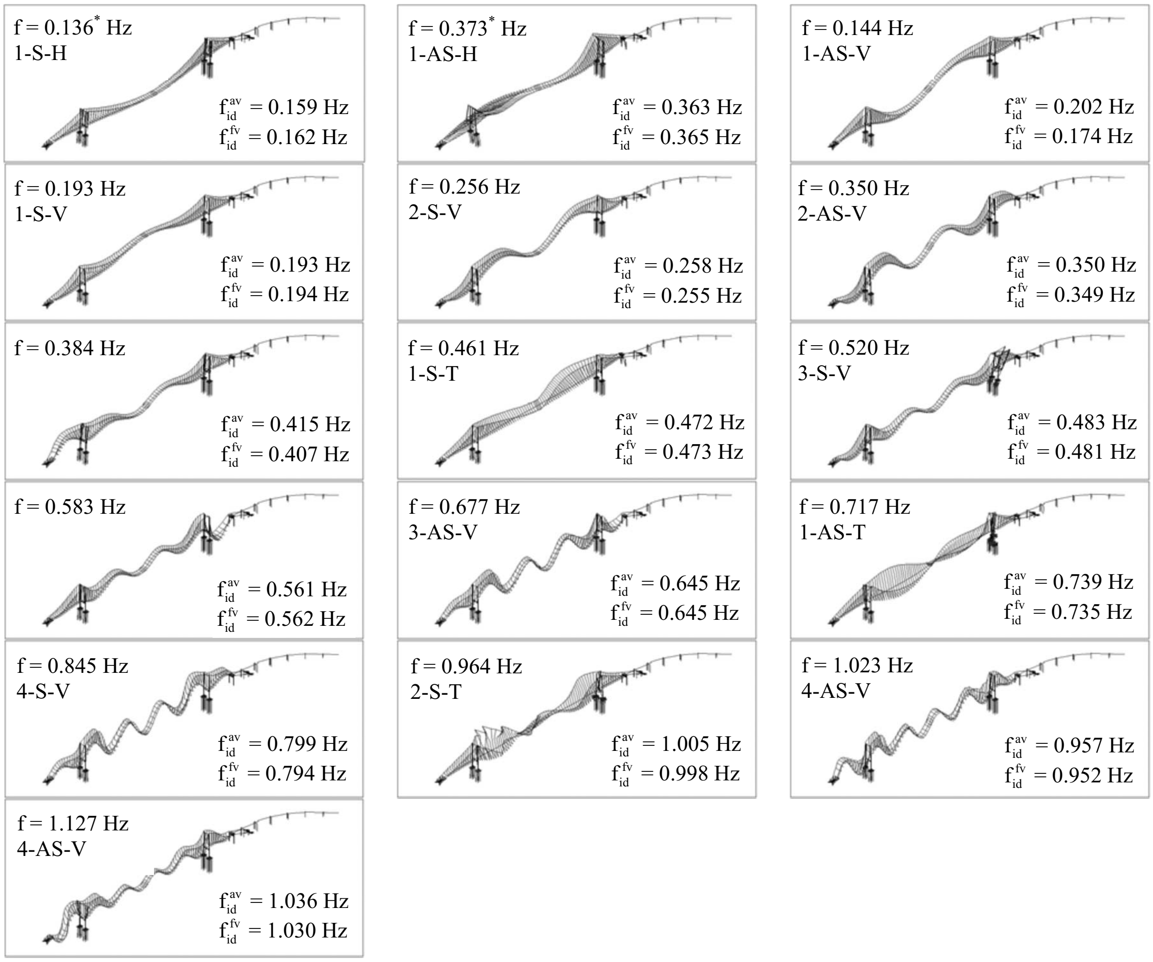


**Fig. 10.** Vibration mode shapes of the AZMB computed from the bridge FE model in ADINA ( *=horizontal vibration modes and $f_{id}^{av}, f_{id}^{fv}$ =natural frequency identified based on ambient vibration and forced vibration data, respectively, averaged over the three system identification methods)

damping ratios identified over three methods using forced vibration data are higher than those identified using ambient vibration data; and (5) for most vibration modes, the mode shapes identified using different methods and the different test data are in excellent agreement.

The system identification results obtained from this study provide benchmark modal properties of the AZMB, which can be

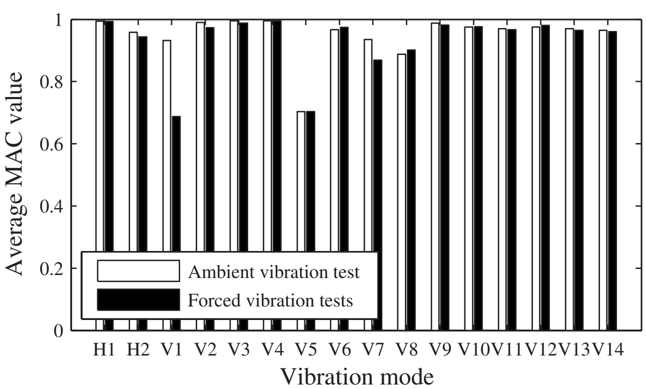


**Fig. 11.** Averaged (over the three methods) MAC values between identified and analytically predicted mode shapes

used as a baseline in future health monitoring studies of this bridge. From the facts that (1) very different methods provide similar results for the modal parameters of the modes contributing most to the measured bridge vibration; (2) the natural frequencies and mode shapes identified using two different types of test data are in good agreement; and (3) these methods were found in a recent study by the writers to provide modal parameter estimates with low bias and variability for the natural frequencies and mode shapes, it can be concluded that it is likely that the identified natural frequencies and mode shapes are close to the actual modal parameters of this bridge. Although the damping ratio estimates provided by this study have a much larger variability across methods (than the natural frequencies and mode shapes), the average values over the three methods are likely to be representative of the actual effective damping ratios of the bridge at the two levels of response amplitude considered.

Overall, all three system identification methods applied in this study performed very well in both types of test. However, use of several system identification methods is recommended for cross-validation purposes and for avoiding missing modes, as different methods provide modal parameter estimators with different intramethod and intermethods statistical properties (bias, variance, covariance), which depend on the frequency content of the input excitation and the level of violation of the assumed amplitude stationarity. It should be noted that the performance of the EFDD method is not as robust as that of the other two methods, as it requires user intervention for peak picking in the identification process.

Finally, the identified natural frequencies and mode shapes are compared with their analytically predicted counterparts obtained from a 3D FE model used in the design phase of the AZMB. The identified (experimental) and analytical modal properties are found to be in good agreement for a few contributing modes to the measured bridge vibration. It should be noted that in the context of this work no calibrated FE model of the bridge was available and that FE model calibration (including revision of modeling assumptions), a significant task by itself, was not in the scope of this study. However, the writers believe that this was a unique opportunity (of interest to the profession) to compare natural frequencies and mode shapes carefully identified experimentally with those computed from a FE model developed for designing the bridge and which therefore had not been modified artificially (fudged) in order to match some measured modal properties. The authors believe that the best approach to reliably identify the actual modal properties of the bridge is through an integrated analytical–experimental approach, updating FE model parameter values and modifying modeling assumptions until an acceptable and optimum match is obtained between the set of identified modal parameters and their FE computed counterparts. This process would have to also account for the estimation uncertainty of the identified modal parameters. This is a very interesting topic of future research work that was not in the scope of this study.

## Acknowledgments

Support of this research by the National Science Foundation under ITR Grant No. 0205720 is gratefully acknowledged. The dynamic field tests on the Alfred Zampa Memorial Bridge (used in this study) were performed by a joint UCSD-USC-UCLA research team. The writers wish to acknowledge the USC and UCLA research team members: John P. Caffrey, Farazad Tasbihgoo, and Mazen Wahbeh (USC), and Steve Kang and Daniel Whang (UCLA) for their cooperation and help during the tests. The writers are grateful to the California Department of Transportation and Dr. Charles Sikorsky who provided the FE model of the AZMB used in this study. Finally, the writers are thankful to Dr. Mark Ketchum (from OPAC Consulting Engineers) for very useful and interesting discussions about the conception and design of the Alfred Zampa Memorial Bridge. Any opinions, findings, and conclusions or recommendations expressed in this material are those of the authors and do not necessarily reflect those of the sponsor.

## References

ADINA R&D, Inc. (2002). "Theory and modeling guide Vol. 1: ADINA." *Rep. No. ARD 02-7*, Watertown, Mass.

Allemang, R. J., and Brown, D. L. (1982). "A correlation coefficient for modal vector analysis." *Proc., 1st Int. Modal Analysis Conf. (IMAC)*, 110–116, Orlando, Fla., Soc. Experimental Mechanics, Inc., Bethel, Conn.

Brincker, R., Ventura, C., and Andersen, P. (2001). "Damping estimation by frequency domain decomposition." *Proc., 19th Int. Modal Analysis Conf. (IMAC)*, Kissimmee, Fla., Soc. Experimental Mechanics, Inc., Bethel, Conn.

Brincker, R., Zhang, L., and Andersen, P. (2000). "Modal identification from ambient responses using frequency domain decomposition." *Proc., 18th Int. Modal Analysis Conf. (IMAC)*, San Antonio, Tex., Soc. Experimental Mechanics, Inc., Bethel, Conn.

Brown, D. L., Allemang, R. J., Zimmerman, R., and Mergeay, M. (1979). "Parameters estimation techniques for modal analysis." *Society of Automotive Engineers (SAE) Technical Paper Series, No. 790221*, Vol. 88, 828–846.

Caicedo, J. M., Dyke, S. J., and Johnson, E. A. (2004). "Natural excitation technique and eigensystem realization algorithm for phase I of the IASC-ASCE benchmark problem: Simulated data." *J. Eng. Mech.*, 130(1), 49–60.

Conte, J. P., et al. (2008). "Dynamic testing of Alfred Zampa Memorial Bridge." *J. Struct. Eng.*, 134(6), 1006–1015.

Farrar, C. R., and James, G. H., III. (1997). "System identification from ambient vibration measurements on a bridge." *J. Sound Vib.*, 205(1), 1–18.

Fukuzono, K. (1986). "Investigation of multiple-reference Ibrahim time domain modal parameter estimation technique." MS thesis, Dept. of Mechanical and Industrial Engineering, Univ. of Cincinnati, Cincinnati.

He, X., Moaveni, B., Conte, J. P., and Elgamal, A. (2006). "Comparative study of system identification techniques applied to New Carquinez Bridge." *Proc., 3rd Int. Conf. on Bridge Maintenance, Safety and Management*, P. J. S. Cruz, D. M. Frangopol, and L. C. Neves, eds., Porto, Portugal, Taylor & Francis, London.

Ibrahim, S. R., and Mikulcik, E. C. (1977). "A method for the direct identification of vibration parameters from the free response." *Shock Vib. Bull.*, 47(4), 183–198.

James, G. H., Carne, T. G., and Lauffer, J. P. (1993). "The natural excitation technique for modal parameters extraction from operating wind turbines." *Rep. No. SAND92–1666*, UC-261, Sandia National Laboratories, Sandia, N.M.

Juang, J. N., and Pappa, R. S. (1985). "An eigensystem realization algorithm for modal parameters identification and model reduction." *J. Guid. Control Dyn.*, 8(5), 620–627.

Moaveni, B., Barbosa, A. R., Conte, J. P., and Hemez, F. M. (2007). "Uncertainty analysis of modal parameters obtained from three system identification methods." *Proc., Int. Conf. on Modal Analysis (IMAC-XXV)*, Orlando, Fla., Soc. Experimental Mechanics, Inc., Bethel, Conn.

Peeters, B., and De Roeck, G. (1999), "Reference-based stochastic subspace identification for output-only modal analysis." *Mech. Syst. Signal Process.*, 13(6), 855–878.

Van Overschee, P., and De Moor, B. (1996). *Subspace identification for linear systems: Theory—Implementation—Applications*, Kluwer Academic, Norwell, Mass.

Vold, H., Kundrat, J., Rocklin, G. T., and Russel, R. (1982). "A Multi-input modal estimation algorithm for mini-computers." *Society of Automotive Engineers (SAE) Technical Paper Series, No. 820194*, Vol. 91, 815–821.